ELSEVIER

Materials Chemistry and Physics 77 (2002) 704–710

MATERIALS CHEMISTRY AND PHYSICS

www.elsevier.com/locate/matchemphys

Ceria-modified zirconia and their effects on the molybdenum oxide dispersion

Zinab A. Omran, Mohamed M. Mohamed*

Chemistry Department, Faculty of Science, Benha University, Benha, Egypt

Received 5 July 2001; received in revised form 23 January 2002; accepted 22 February 2002

Abstract

The CeO_2-modified ZrO_2 support was impregnated in an aqueous solution of ammonium heptamolybdate to achieve a loading of 8 wt.% Mo. This material (Mo/Zr(Ce)) was characterized, in comparison with Mo/Zr, by X-ray diffraction, FT-IR and UV–VIS diffuse reflectance spectroscopy as well as low temperature N_2 adsorption and electrical conductivity measurements. The X-ray results showed that the particles size of MoO_3 on Zr(Ce) (24.7 nm) was lower than those on ceria free Zr (36.7 nm). The IR results indicated that a strong interaction between Mo species and zirconia was recognized in the Mo/Zr(Ce) sample by the appearance of a new band at 858 cm^{-1} attributed to a Mo–O–Zr linkage, which was not detected in the Mo/Zr sample. The UV–VIS spectra showed that both octahedral (291 nm) and tetrahedral (249 nm) Mo^{6+} were detected in the Mo/Zr sample where tetrahedral arrangement (246 nm) was only adopted for Mo^{6+} in the Mo/Zr(Ce) sample. The addition of either Ce or Mo to zirconia causes a marked increase in the specific surface area of the samples. The conductivity measurements showed that all samples exhibit a semiconducting behavior.
© 2002 Elsevier Science B.V. All rights reserved.

Keywords: Molybdenum; Zr(Ce); Structure; Texturing; Anionic conduction

1. Introduction

Molybdenum oxide based catalysts are considerably attracted much attention of many researchers because of their wide applications in petroleum refining, chemicals production and pollution control industries [1–3]. These catalysts are belonging to those used for oxidation and ammoxidation reactions [4,5], which perceived a renewed interest depending on the going rate of achieving dispersion of MoO_3 in a catalyst support. On the other hand, the composition of the support, its exposed phase, surface area and surface acidity play a very important role for optimizing the performance of supported molybdenum towards specific reactions. Until recently, most of the research work was focused on alumina as well as silica supported molybdenum [6–8]. Supports other than alumina and silica, e.g. titania, titania–silica, zirconia and titania–zirconia, have received less attention [9–12].

Zirconia is found to be the favored support for sulfided Mo catalysts that exhibited excellent catalytic properties for hydrodesulfrization of thiophen [13]. Although, the acknowledged unique catalytic, acidic, basic oxide and reducing properties of ZrO_2 [14], it appears that the most challenge putting it in service as a support is its typical small surface area in addition to lowering both thermal and mechanical stabilities. Accordingly, minimizing the sintering of zirconia on one hand and enhancing the mechanical properties on the other hand besides, increasing its surface area was accomplished through the combination with other supports, e.g. TiO_2–ZrO_2 [10] and SiO_2–ZrO_2 [15]. These combined mixed oxides of special tailored properties altered the chemisorptive properties of ZrO_2 through modifying its nature and composition [10,12,15].

Doping the ZrO_2 support with cerium containing materials can lead to such alterations because of the ability of the latter to create surface and bulk vacancies counting on the generation of Ce^{3+}/Ce^{4+} redox couple [16]. Previous studies have shown that adding ZrO_2 to CeO_2 enhances the stability of CeO_2 particles against thermal sintering [17,18]. There have been limited investigations on the phase diagram of the ceramic system CeO_2–ZrO_2, which was characterized by the high electron conductive and mechanical properties [19,20]. Through the surface vacant sites created on ceria support, an achieved high dispersion of MoO_3 species was attained [21]. Because of favorable characteristics of the combined CeO_2–ZrO_2 system, it can be used as a support for molybdenum catalysts. Thus, this work focuses on the consequences of adding ceria into zirconia

* Corresponding author.
E-mail address: mohmok2000@yahoo.com (M.M. Mohamed).

0254-0584/02/$ – see front matter © 2002 Elsevier Science B.V. All rights reserved.
PII: S0254-0584(02)00170-0

and their effects toward the dispersion capacity of MoO_3 besides, providing basic insights into the surface structure of the $Mo/ZrO_2(CeO_2)$ system. In this investigation, X-ray diffraction, FT-IR, UV diffuse reflectance and BET surface area measurements were employed to examine the structure, phases, surface molybdates and interactions among the phases of the catalysts. An overview about the dc conductivity of the samples was also presented for providing more practical understanding of the studied catalysts.

2. Experiment

The parent zirconia carrier (ZrO_2), used in the present study of surface area (BET) 220 $m^2\,g^{-1}$, was used as received (BDH). To prepare CeO_2 doped ZrO_2 carrier, weighed amount of ZrO_2 and Ce $(NO_3)_3{\cdot}6H_2O$ (Strem Chemicals, 99.99%), so as to yield 1 wt.% CeO_2/ZrO_2, was slurried with distilled water and thoroughly mixed. The water was evaporated under continuous stirring and the residue was dried at 393 K for 12 h and then calcined at 773 K for 16 h. The 8 wt.% Mo/ZrO_2 and Mo/ZrO_2(Ce) samples were prepared by the method of incipient wetness impregnation using ammonium heptamolybdate $(NH_4)_6Mo_7O_{24}{\cdot}4H_2O$ (Fluka, AR grade) solution (at pH 6.0). These samples were referred to as Mo/Zr and Mo/Zr(Ce), respectively. The samples were dried at 393 K for 12 h, and finally calcined at 773 K for 16 h. The concentration of heptamolybdate (8 wt.%) was that required to not only cover the support surface by a compact single lamella of molybdenum oxide structure but also go beyond this value [10]. This was undertaken to investigate the extent of the dispersion of MoO_3 over the modified and non-modified ZrO_2 support.

X-ray powder diffraction patterns were recorded in a Philips 321/00 instrument using Ni-filtered Cu Kα radiation ($\lambda = 1.541$ Å). The XRD phases present in the samples were identified with the help of ASTM powder data files.

The FT-IR spectra were recorded on a Bruker (Vector 22) single beam spectrometer at ambient conditions using KBr disks, with nominal resolution of 2 cm^{-1}. The measurements were recorded at room temperature in the range of 1100–450 cm^{-1}.

UV–VIS diffuse reflectance spectra of various samples in the 500–200 nm range were obtained using a Jasco V-570 (serial number, C29635) spectrophotometer, which was attached to a diffuse reflectance accessory.

A conventional standard volumetric high vacuum (10^{-5} Torr) system was used to obtain the N_2 adsorption–desorption isotherms at 77 K. The samples were outgassed at 473 K for 3 h before starting the run. A highly pure (99%) N_2 gas is used as adsorbate.

The dc electrical conductivity measurements were carried out on the samples in the form of pellets of diameter 7 mm and thickness of about 1 mm, prepared by pressing the samples powder under a pressure of 2×103 kg cm^{-2}. The two parallel surfaces of the pellet were coated with silver paste (BDH) to ensure good electrical contact during the measurement using the two-probe method. The pellet was located in a sample holder and measured under air atmosphere in the temperature range 298–723 K at temperature intervals of 20 K. The temperature was controlled using an Oxford temperature controller.

3. Results and discussion

3.1. X-ray diffraction

Fig. 1 shows the XRD patterns of ceria modified zirconia and ceria free zirconia when supported by molybdenum catalysts in comparison with the pattern of ceria modified zirconia, all calcined at 773 K. The latter pattern generally shows three phases: CeO_2, ZrO_2 and (Zr, Ce)O_2. The CeO_2 phase exhibited strong peaks corresponding to $d = 3.10$ and 1.91 Å for (1 1 1) and (2 2 0) faces, respectively, of the cubic structure. Whereas, the ZrO_2 phase showed a strong peak corresponding to $d = 2.92$ Å characterizing of the (1 1 1) face of tetragonal structure. The (Zr, Ce)O_2 phase showed broad peaks at $d = 2.59$ and 1.89 Å in addition to another one at $d = 1.84$ Å. These peaks were similar to those identified by Yao et al. [22] who established the formation of the solid solution $Zr_xCe_{1-x}O_2$ phase of cubic symmetry on alumina support. Thus, we tentatively attributed the latter peaks to the $Zr_xCe_{1-x}O_2$ phase.

The XRD pattern of the Mo/Zr sample revealed the absence of the main peak characteristics of the ZrO_2 support ($d = 2.92$ Å) in favor of the production of $ZrMo_2O_8$ (e.g. $d = 2.70$, 2.35, 1.69 and 1.67 Å) and MoO_3 ($d = 6.93$, 3.81 and 3.26 Å) phases. Comparison of this pattern with that of ceria modified zirconia containing the same Mo loading pointed out marked variations. A high dispersion of crystalline molybdenum was accomplished on ceria-modified zirconia (24.7 nm, as determined by Scherrer equation) rather than on the corresponding non-modified (36.7 nm). This was paralleled to the generation of two strong peaks at $d = 3.14$ and 2.82 Å corresponding to the (1 1 1) face of monoclinic ZrO_2. In addition, diminishing the intensity of some $ZrMo_2O_8$ lines (e.g. $d = 1.69$ and 1.67 Å) and vanishing of some others (e.g. $d = 2.35$ and 1.89 Å) were obtained. This indicates that the presence of CeO_2 on ZrO_2 was responsible for the MoO_3 dispersion that tentatively ascribed to surface vacant sites created by ceria upon doping with zirconia. The domination of the monoclinic ZrO_2 on the surface of Mo/Zr(Ce) rather than the tetragonal one, exhibited on Zr(Ce), could be a consequence of the high dispersion of MoO_3. The absence of the (1 1 1) diffraction line of ceria upon Mo incorporation indicated that Mo species were preferably located in the vicinity of this site. The exhibited decrease and broadening of some $ZrMo_2O_8$ lines in the pattern of Mo/Zr(Ce) sample as well as vanishing of some others provided an evidence for the dispersion and diminishing the crystallites size of this phase. The average

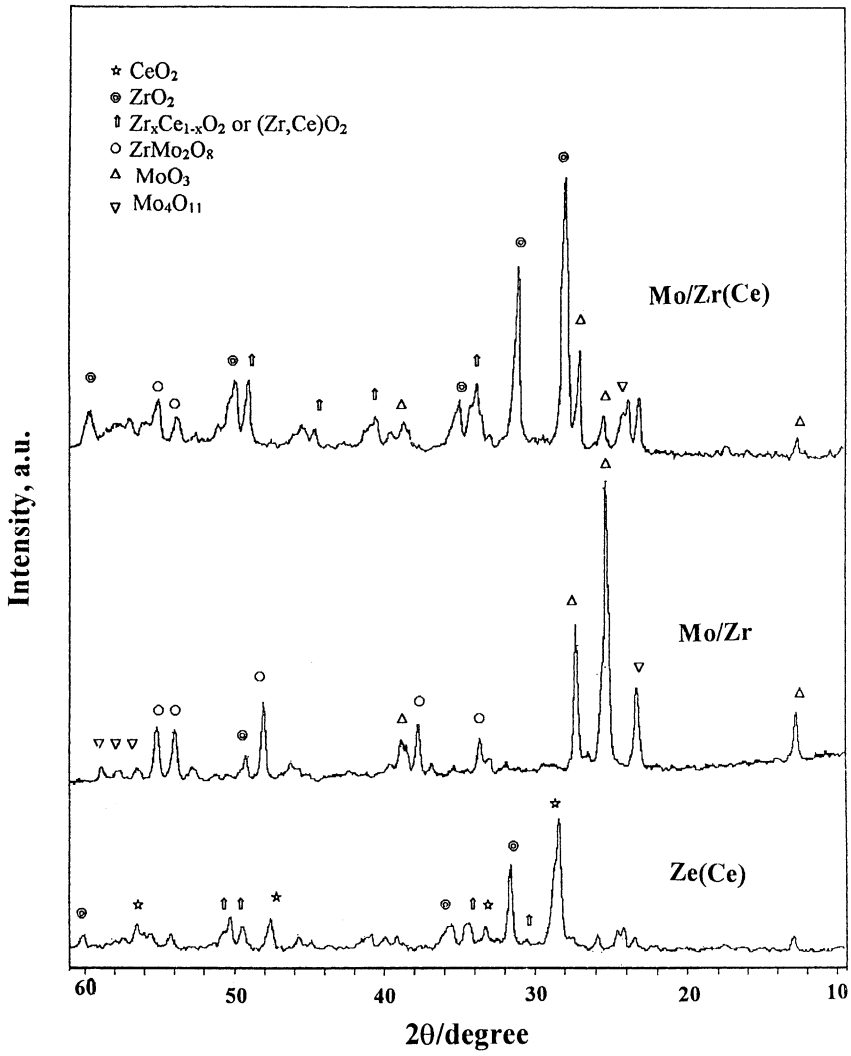

Fig. 1. X-ray diffraction patterns of Zr(Ce), Mo/Zr and Mo/Zr(Ce) catalysts calcined at 773 K.

particle size of $ZrMo_2O_8$ in the latter sample was 19.7 nm, as determined by Scherrer equation, which was considerably lower than that in Mo/Zr (27.8 nm). This indicates that the presence of CeO_2 inhibits the sintering possibility of $ZrMo_2O_8$ phase.

3.2. Infrared spectroscopy

The IR spectrum of ceria-modified zirconia (calcined at 773 K) (Fig. 2) displays strong absorption bands at 758, 655, 587 cm^{-1} besides, two bands at 500 and 453 cm^{-1} characteristic, respectively, of stretching vibrations of Zr–O bonds of varying covalent character and Ce–O lattice vibrations [23,24]. The IR spectrum of the Mo/Zr sample is characterized by the substantial removal of some vibrational bands of ZrO_2, for example, 758 and 655 cm^{-1}. This indicates that a strong interaction between molybdenum species and the ZrO_2 support was formed. The formation of surface polymolybdate was revealed by the band at 876 cm^{-1}, due to ν_{as} (Mo–O–Mo), in addition to a strong band at 993 cm^{-1} ascribed to Mo–O_t stretching vibration in crystalline MoO_3 [7,8]. The small band at 816 cm^{-1} can be attributed to the bulk oxide attached to Mo–O–Mo vibrations. Frausen et al. [25] reported that heating ZrO_2 with MoO_3 at 820 K provokes the formation of the $ZrMo_2O_8$ compound that showed IR bands at 980, 920 and 800 cm^{-1}. By virtue, our IR results can give an evidence for the formation of the latter compound in spite of the expected interference with polymolybdate and octahedral oxomolybdenum species. The bands at 993 and 816 cm^{-1}, in the Mo/Zr spectrum, are matching those at 980 and 800 cm^{-1}, respectively, in the latter compound. A remnant shoulder at 960 cm^{-1}, that can hardly be seen was also ascribed to the $ZrMo_2O_8$ compound, as has been reported by others [26].

The small band at 1066 cm^{-1} was attributed to covering ZrO_2 surface by a single monolayer of Mo. This assignment was in agreement with the IR results of the MoO_3/CeO_2 catalyst, which showed a prominent band at 1050 cm^{-1} [21].

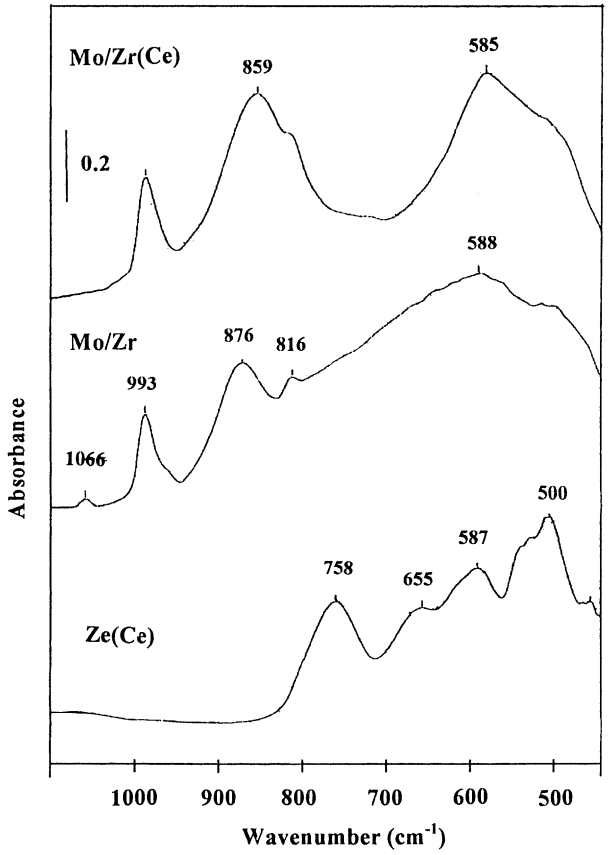

Fig. 2. FT-IR spectra of Zr(Ce), Mo/Zr and Mo/Zr(Ce) catalysts calcined at 773 K.

Increasing facts for this assignment comes from the following: firstly, this band was not apparent in the spectrum of ceria-modified zirconia, indicating that it does not belong to any of these oxides. Secondly, this band is not characteristic of $ZrMo_2O_8$ because it's out the margin of these compound bands.

The spectrum of the Mo/Zr(Ce) sample showed absorption bands at 993, 859, 816_{sh}, 725_{sh}, 584 and 510_{sh} cm^{-1}. This spectrum is characterized by new bands at 859 and 725_{sh}, if compared with that of Mo/Zr. The latter bands are due to the formation of $ZrMo_2O_8$ compound. The privilege of this compound can be inferred from the presence of the Mo–O–Zr linkage at 859 cm^{-1} that was not indicated by the spectrum of Mo/Zr sample [27]. Hence, the interaction between MoO_3 and ZrO_2 was stronger with the presence of CeO_2. As a result of this interaction, the bands at 875 and 816 cm^{-1}, seen in the spectrum of the Mo/Zr sample, were vanished and markedly decreased in intensity, respectively, in the spectrum of the Mo/Zr(Ce) sample. It appears that CeO_2 affects the particles size of ZrO_2 to be eligible for the interaction with MoO_3 so as to forming Mo–O–Zr linkages and hence diminishing the polymolybdate, ν(Mo–O–Mo) in MoO_3, species [28]. This suggests the improvement of MoO_3 dispersion. In conclusion, $ZrMo_2O_8$ is more favored by the presence of CeO_2, probably due to its effect in increasing the dispersion of Mo species; as has been evidenced by XRD results. An additional reason could be due to lowering the temperatures of ZrO_2 formation than those of MoO_3 upon introducing CeO_2. Generally, it seems that the spinel $ZrMo_2O_8$ was formed by the diffusion action of Mo-ions into ZrO_2 through the facility purchased by CeO_2.

3.3. UV–VIS diffuse reflectance spectroscopy

The UV–VIS diffuse reflectance spectra of Mo/Zr and Mo/Zr(Ce) samples were collected in Fig. 3 together with the spectra of the reference samples, Zr and Zr–Ce. The spectrum of Mo/Zr sample showed a very intense narrow band at 208 nm and two small ones at 217 and 228 nm. Besides, bands at 240, 250, 291 and 333 nm were also observed. The former bands were similar to those obtained for Zr–Ce but of lower intensities. The bands at 250, 291 and 333 nm gave information on the nature and coordination of Mo^{6+}-ions on zirconia, via the charge transfer transition $O^{2-} \rightarrow Mo^{6+}$, where Mo^{6+}-ions in tetrahedral coordination occurred at

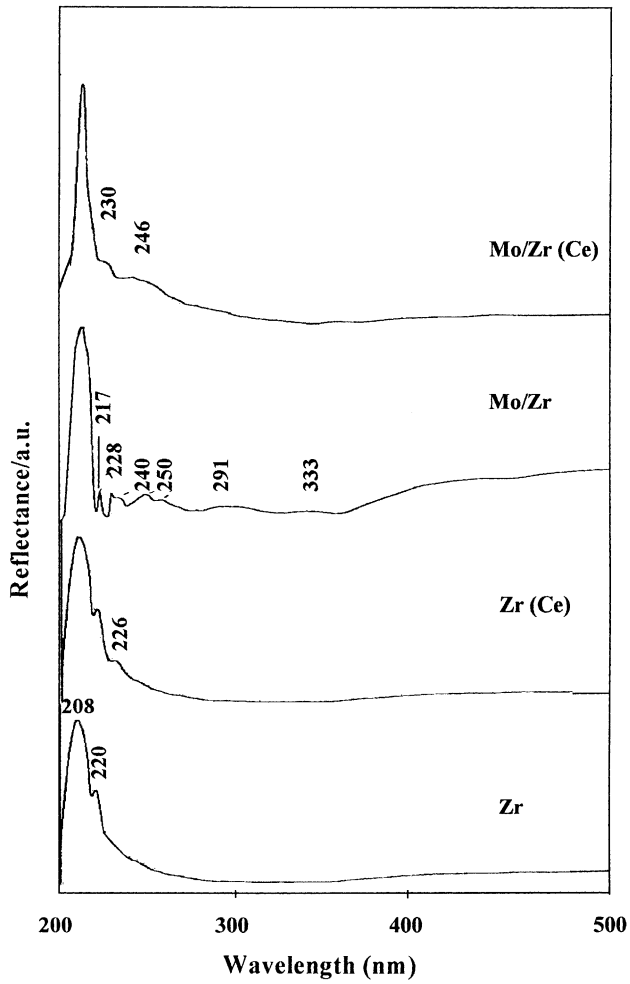

Fig. 3. UV–VIS spectra of Zr, Zr(Ce), Mo/Zr and Mo/Zr(Ce) catalysts calcined at 773 K.

shorter wavelengths (250 nm) than those in octahedral coordination (291 and 333 nm) [29]. This indicates that the dominant species were Mo^{6+}-ions in octahedral coordination. The band at 240 nm was indicative of the presence of Zr atoms, which are likely isolated, in an octahedral coordination. This agrees with the data of Lever [30] on ZrO_2, which suggested the octahedral coordination of Zr atoms through the involvement of two water molecules in the coordination sphere.

On the other hand, the spectrum of Mo/Zr(Ce) sample showed bands at 208 and 230 nm, which were similar to those in Zr(Ce), together with a broad band at 246 nm. It appears that Ce modified the support ZrO_2 to be suitable for only exposing Mo^{6+} in four-fold coordination (246 nm). This gives a clue about the high dispersion Mo-ions in the latter sample, which revealed no bands characteristic of MoO_3, if compared with the Mo/Zr sample. This result was in agreement with that obtained from X-ray and IR data of the samples.

Inspection of the spectra of Fig. 3 indicated the presence of a broad band around 400 nm in Mo/Zr sample. This band can not be due to a $Mo^{6+} \rightarrow Zr^{4+}$ charge transfer because of the forbidden d–d transition of Mo^{6+}-ions (d^0) i.e. no d electron could be promoted to the conduction band of ZrO_2. The origin of this band could be correlated with the formation of a new oxygen containing species [31] on the surface of zirconia stabilized by Mo-ions.

The enhanced width of band maximized at 208 nm in the spectra of Zr(Ce) and Zr samples rather than that in the spectrum of Mo/Zr(Ce) sample can be due to the presence of defect sites in the former samples that perform contribution with Mo yielding the narrow width action in the latter sample. This result was in agreement with that of Trongon et al. [32] who confirmed the presence of defect sites in the silicate framework as a result of its association with titania.

3.4. N_2 adsorption

The various surface characteristics, i.e. specific surface area (S_{BET}), total pore volume (V_p), BET C-constant, and the average pore radius (r_H), which were determined from nitrogen adsorption isotherms (77 K) for the samples, are given in Table 1. Inspecting the data in this Table, we can note that an increase in S_{BET} is produced upon either the addition of Ce or Mo on zirconia support. Concurrently, a significant decrease in r_H was produced that paralleled to almost no change in V_p. The change in the specific surface area was found in the following order, Mo/Zr > Mo/Zr–Ce > Zr–Ce > Zr. The increase in S_{BET} of zirconia due to treatment with Ce, i.e. Zr–Ce, could be due to creation of new pores produced from the departure of NO_x compounds during the thermal treatment of cerium nitrate. As another plausible explanation, at 773 K, X-ray analyses revealed the formation of the $Zr_xCe_{1-x}O_2$ phase of pore narrowing character and thus, rendering the surface microporosity, i.e. micropores are characterized by a high surface area. The marked increase in S_{BET} for Zr and Zr(Ce) samples due to treatment with 8 wt.% Mo can be attributed to the formation of $ZrMo_2O_8$ spinel, i.e. new pores having their own micropores character.

It is clear from Table 1 that S_{BET} and S_t are close to each other, thereby indicating the absence of ultramicropores in the samples. A more emphasize on the pore structure was achieved through constructing the V_l–t plots in which the t curves of Lacloux and Pirard [33] are used, depending on the value of the BET C constant. The correct choice of the

Table 1
Surface characteristics of the studied samples

Sample	S_{BET} ($m^2\,g^{-1}$)	S_T ($m^2\,g^{-1}$)	V_p ($ml\,g^{-1}$)	R_H (Å)	C_{BET}
Zr	220	217	0.41	37.2	19
Mo/Zr	433	392	0.37	17.1	25
Zr(Ce)	300	316	0.41	27.3	22
Mo/Zr(Ce)	414	433	0.37	17.8	28

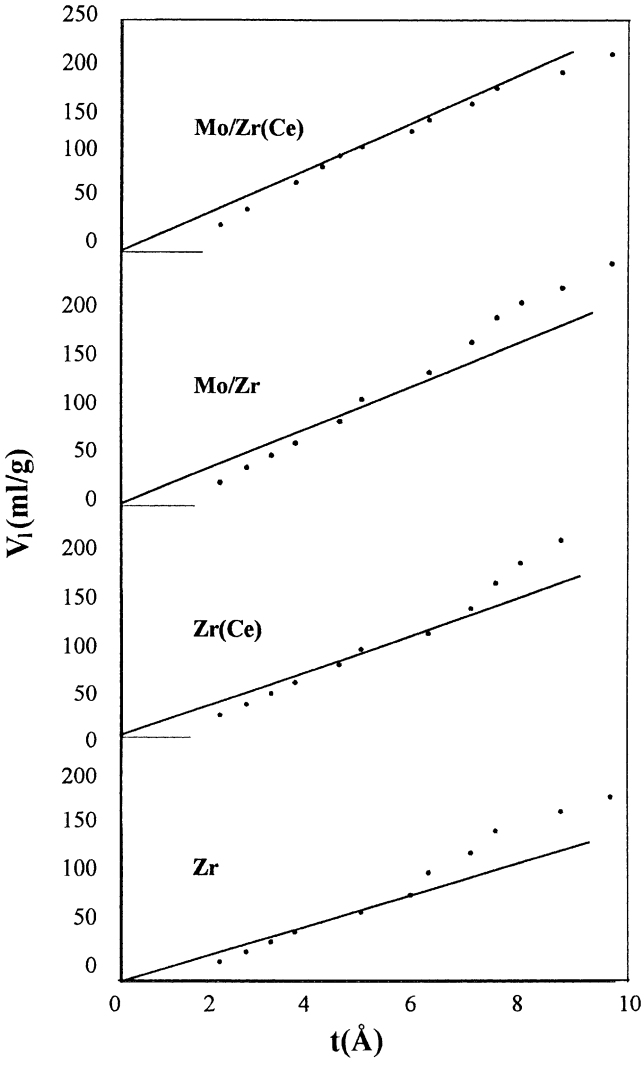

Fig. 4. V_l–t plots of Zr, Zr(Ce), Mo/Zr and Mo/Zr(Ce) catalysts.

reference t values is verified through the agreement between the area calculated from the plot, S_t, and S_{BET} (Table 1).

The obtained V_l–t plots (Fig. 4) of Zr, Zr–Ce and Mo/Zr samples exhibited a similar trend. They indicated generally a mesoporous structure, as observed from the corresponding upward deviations. These deviations are observed at a relative pressure values $p/p^0 = 0.5$, 0.62 and 0.5, respectively. This governs the arrangement of wide pores to be in the order Zr = Mo/Zr > Ze(Ce). It seems then for the Zr(Ce) sample that Ce has consumed most of the pores of wider sizes and left behind a slight downward deviation. This reflects the heterogeneity of the sample texture. The latter phenomenon was typically occurred in the Mo/Zr sample probably because of the interaction that favored the formation of spinel $ZrMo_2O_8$ of absolutely narrow pores nature. This has been manifested by presence of some points in the t range 3.6–4.5 Å ($p/p^0 = 0.2$–0.35), which lie just down the straight line extended to pass through origin before the start of the upward deviation at $t = 6.0$ Å. The size of this downward deviation indicates the presence of a number of pores of sizes in the lower limit of micropores. In contrast, the V_l–t plot of Mo/Zr(Ce) sample appears to possess a texture dominated by micropores if compared with that derived from the Mo/Zr plot, where the start of the downward deviation in the V_l–t plot at $t = 7.5$ Å ($p/p^0 = 0.68$). This approximately matched the hysteresis closure point at $p/p^0 = 0.65$ in the corresponding adsorption isotherm (not shown). Thus, it seems that the addition of Mo resulted in blocking of finer pores and narrowing of wider ones and further proceeded in the construction of separate phase of $ZrMo_2O_8$, which was responsible for the character of microporosity.

3.5. Electrical properties

The temperature dependence of electrical conductivity in the temperature range from 298 to 723 K for MoO_3, ZrO_2, Zr–Ce, Mo/Zr and Mo/Zr(Ce) samples are shown in Fig. 5. The conductivity for all samples was shown to increase with temperature. The electrical conductivity of ceria modified Zr was higher than that of pure ZrO_2. This was probably due to the dissolution of both oxides in each other forming the $Zr_xCe_{1-x}O_2$ phase that characterized by its ionic conductivity, i.e. fluorite structure [34,35]. The enhancement in conductivity was attributed to increasing the concentration of oxygen vacancies as a result of dissolving Ce^{3+}-ions in ZrO_2 causing varied lattices of CeO_2 in ZrO_2 with temperatures. In the Mo/Zr sample, the increase in conductivity was attributed to higher conduction of spinel $ZrMo_2O_8$ [36].

On comparing the electrical conductivity of Zr(Ce) and Mo/Zr(Ce) samples, it can be observed that the former

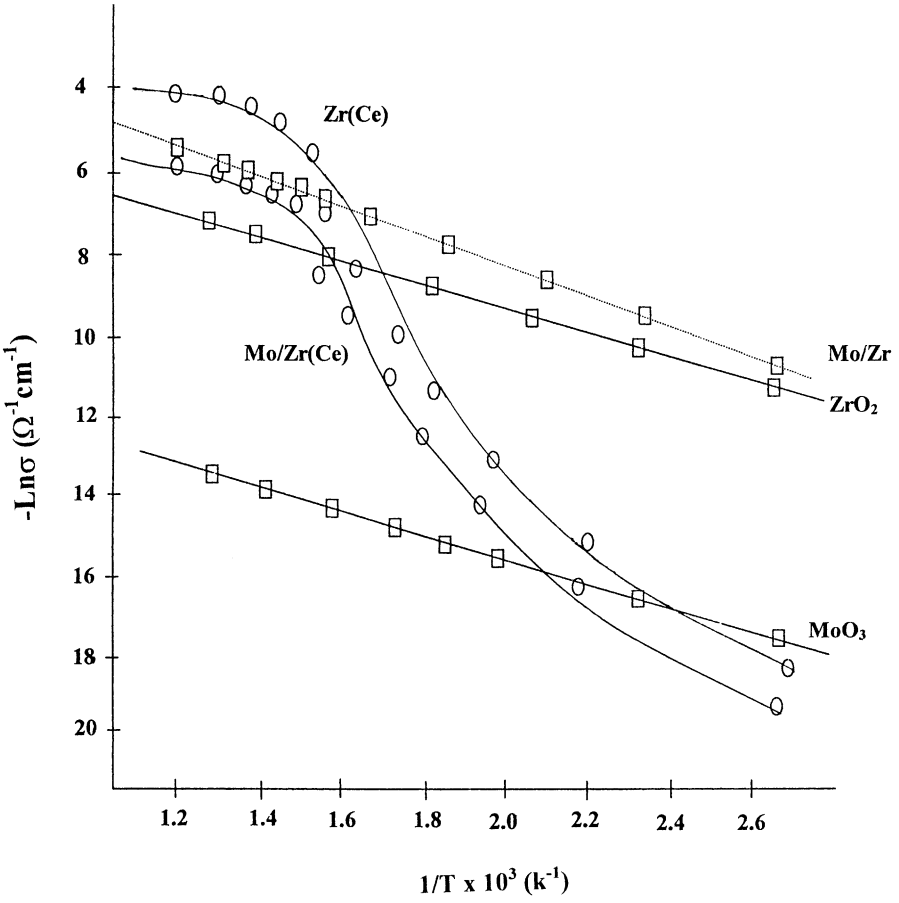

Fig. 5. Temperature dependence of the electrical conductivity for ZrO_2, MoO_3, Zr(Ce), Mo/Zr and Mo/Zr(Ce) catalysts.

sample showed higher conduction than that of the latter. In other words, the addition of Mo^{6+} to cerium modified zirconia has produced a decrease in the conductivity values of the Zr(Ce) sample. This can qualitatively be discussed as follows; it is greatly believed that the introduction of a foreign ion having a large size into the lattice of a host material would causes a strain in the lattice [37]. Such strain produces lattice distortion and as a result of a change in defects is perceived that in turn perturbs the electric conduction. The significant loss in the conductivity of Mo/Zr sample if compared with Zr(Ce) one was due to anionic and possibly cationic (e.g. Zr^{4+}/Mo^{6+}) exchanges between the two oxides. However, the conductivity curve of the former sample only showed one phase giving a criterion about the involvement of the $ZrMo_2O_8$ phase in its behavior. The two phases observed in the conductivity curve of Mo/Zr(Ce) sample suggests the involvement of two phases in the conductivity of this sample.

4. Conclusions

The following conclusions can be drawn from this study.

The interaction between ZrO_2 and MoO_3 was more facile in Mo/Zr(Ce) sample, rather than that in Mo/Zr, due to the appreciable formation of spinel $ZrMo_2O_8$, which was taken as a measure for the dispersion of MoO_3 species. It has been revealed the respective benefit of adding CeO_2 into ZrO_2 substrate in showing his own advantages on the MoO_3 dispersion. This dispersion was identified and confirmed by IR, XRD and UV–DRS techniques. Specific surface areas as high as 414–433 $m^2\,g^{-1}$ were achieved by adding Mo or Ce, or both, due to the formation of $ZrMo_2O_8$ or $Zr_xCe_{1-x}O_2$ phases, respectively. The latter phases were found to be responsible for enhancing the conductivity of Mo/Zr and Zr(Ce) samples. The $Zr_xCe_{1-x}O_2$ phase that produces lattice defects, such as anionic vacancies, showed unique conductivity behavior comparatively.

References

[1] R. Prins, V.H.J. De Beer, G.A. Somorjai, Catal. Rev. Sci. Eng. 31 (1989) 1.
[2] T. Ono, Y. Nakagawa, H. Miyata, Y. Kubokawa, Bull. Chem. Soc. Jpn. 57 (1984) 1025.
[3] K. Bruckman, B. Grzybowska, M. Che, J.M. Tatibouet, Appl. Catal. A: General 96 (1993) 279 (and references therein).
[4] S.T. Oyama, W. Zhang, J. Am. Chem. Soc. 118 (1996) 7173.
[5] J.S. Chung, R. Miranda, C.O. Bennett, J. Catal. 114 (1988) 398.
[6] L. Roderigo, A. Adivot, P.C. Roberge, S. Kaliaguine, J. Catal. 105 (1987) 175.
[7] M.M. Mohamed, G.M.S. El-Shafei, Spectrochim. Acta 51 (A) (1995) 1525.
[8] G.M.S. El-Shafei, M.M. Mohamed, Colloids Surf. A 94 (1995) 267.
[9] M. Del-Arco, M.J. Holgado, C. Martin, V. Rives, J. Catal. 99 (1986) 19.
[10] B.M. Reddy, B. Chowdhury, J. Catal. 179 (1998) 413.
[11] J. Miciukiewicz, T. Mang, H. Knozinger, Appl. Catal. A 122 (1995) 151.
[12] V.H.J. De-Beer, J.C. Duchet, R. Prins, J. Catal. 72 (1981) 369.
[13] B.M. Reddy, K.V.R. Chary, B.R. Rao, V.S. Subrahmanyam, C.S. Sunandana, N.K. Nag, Polyhedron 5 (1986) 191.
[14] K. Tanabe, Mater. Chem. Phys. 13 (1985) 3479.
[15] H.J.M. Bosman, A.P. Pijpers, A.W.E.M.A. Jaspers, J. Catal. 161 (1996) 551.
[16] A. Trovarelli, C. De Leitenburg, G. Dolcetti, J. Llorca, J. Catal. 151 (1995) 111.
[17] T. Murota, T. Hasegawa, S.J. Aozasa, Alloys Compounds 193 (1993) 298.
[18] L.L. Murrell, S.J. Tauster, in Catalysis and Automotive Pollution Control II, in: A. Crucq (Ed.), Elsevier, Amsterdam, 1991, p. 547.
[19] P. Duwez, F. Odell, J. Am. Ceram. Soc. 33 (1950) 274.
[20] S. Meriani, Mat. Sci. Eng. A 109 (1989) 121.
[21] L. Dong, Y. Chen, J. Chem. Soc. Faraday Trans. 92 (22) (1996) 4589.
[22] M.H. Yao, R.J. Baird, F.W. Kunz, T.E. Hoost, J. Catal. 166 (1997) 67.
[23] I.E. Wachs, Catal. Today 27 (1996) 437.
[24] H.L. Wan, X.P. Zhou, W.Z. Weng, R.Q. Long, Z.S. Chao, W.D. Zhang, M.S. Chem, J.Z. Luo, S.Q. Zhou, Catal. Today 51 (1999) 161.
[25] T. Frausen, P. C. Vanberge, P. Mars, Preparation of Catalysts I.P. 405, Elsevier, Amsterdam, 1976.
[26] P. Tarte, M. Auray, in: Proceedings of The Second European Conference on Solid State Chemistry, Velhoven, The Netherlands, 7–9 June 1982.
[27] R. Metselaar, H.J.M. Heijligers, J. Schoonman (Eds.), Studies In Inorganic Chemistry, Vol. 3, Elsevier, 1986.
[28] M.A. Banares, H. Hu, I.E. Wachs, J. Catal. 150 (1994) 407.
[29] K. Marcinkowska, S. Kaliaguine, P.C. Roberge, J. Catal. 90 (1984) 49.
[30] A. B. P. Lever, Inorganic Electronic Spectroscopy, 2nd Edition, Elsevier, 1984, p. 378.
[31] M. Del Arco, M.J. Holgado, C. Martin, V. Rives, J. Catal. 99 (1986) 19.
[32] D. Trongon, A. Bittar, A. Sayari, S. Kaliaguine, L. Bonneviot, Catal. Lett. 16 (1992) 85.
[33] A. Lacloux, J.P. Pirard, J. Colloid. Interf. Sci. 70 (1979) 265.
[34] Y. Nigara, K. Watanabe, K. Kawamura, J. Mizuski, M. Ishigame, J. Electrochem. Soc. 144 (1997) 1050.
[35] T. Kawada, N. Sakai, H. Yokokawa, M. Dokiya, Solid State Ion. 418 (1992) 53.
[36] R.J. Brook, J. Yee, F.A. Krger, J. Am. Ceram. Soc. 54 (1971) 414.
[37] M. Palanisamy, K. Thangaraj, P. Ramasay, J. Mater. Sci. 21 (1986) 1075.